catalysts

MDPI

Article

Investigation of Iron Vanadates for Simultaneous Carbon Soot Abatement and NH_3-SCR

Marzia Casanova *, Sara Colussi and Alessandro Trovarelli

Dipartimento Politecnico di Ingegneria e Architettura, Università degli Studi di Udine, via Cotonificio 108, 33100 Udine, Italy; sara.colussi@uniud.it (S.C.); trovarelli@uniud.it (A.T.)

* Correspondence: marzia.casanova@uniud.it; Tel.: +39-0432-558-755

Received: 7 March 2018; Accepted: 22 March 2018; Published: 26 March 2018

Abstract: $FeVO_4$ and $Fe_{0.5}Er_{0.5}VO_4$ were prepared and loaded over standard Selective Catalytic Reduction (SCR) supports based on TiO_2-WO_3-SiO_2 (TWS) and redox active supports like CeO_2 and $CeZrO_2$ with the aim of finding a suitable formulation for simultaneous soot abatement and NH_3-SCR and to understand the level of interaction between the two reactions. A suitable bi-functional material was identified in the composition $FeVO_4/CeZrO_2$ where an SCR active component is added over a redox active support, to increase carbon oxidation properties. The influence of the presence of ammonia in soot oxidation and the effect of the presence of soot on SCR reaction have been addressed. It is found that the addition of NO and NO/NH_3 mixtures decreases at different levels the oxidation temperature of carbon soot, while the presence of carbon adversely affects the NH_3-SCR reaction by increasing the oxidation of NH_3 to NO, thus lowering the NO removal efficiency.

Keywords: NH_3-SCR; soot oxidation; de-soot/deNO_x; $FeVO_4$; Titania; Ceria

1. Introduction

The study of Diesel exhaust after-treatment technologies is focusing on one side in finding novel formulations for active soot oxidation [1] and de-NO_x catalysts [2–4] and on the other side in looking for suitable strategies to limit the number of different process units and combine more functionalities in one single step [5]. Nowadays, the mobile exhaust gas after-treatment is comprised of a series of stand-alone devices, starting from an oxidation catalyst (DOC), a diesel particulate filter (DPF) and a de-NO_x reactor which includes a NO_x storage/reduction system or, alternatively, a NH_3-SCR (Selective Catalytic Reduction) unit. Among the NO_x removal technologies, Selective Catalytic Reduction with NH_3 (NH_3-SCR) has been successfully employed both in stationary and heavy duty mobile applications [6].

Increasingly restrictive limitations concerning emissions of nitrogen oxides and soot particulates from vehicle engines will demand the simultaneous application of a particulate filter and a SCR de-NO_x system. The motivation for the integration of the two reactions is to obtain a reduction of cost and volume of the engine after-treatment system via inclusion of SCR and DPF functionalities into a single entity. Different bi-functional configurations are possible with DPF and SCR catalyst placed in the same housing [7], or with a DPF filter coated with an SCR catalyst formulation [8–10].

The aim of this work is to study the behaviour of a suitable catalyst with acceptable performances both in soot oxidation and in the NH_3-SCR reaction conducted simultaneously. For this purpose, an active SCR catalyst formulation has been loaded over supports showing different soot oxidation functionalities. SCR catalyst materials were selected among metal/rare earth vanadates that have been shown to act as efficient catalyst precursors for NH_3-SCR reaction [11–16], while among the different supports, standard TiO_2-WO_3-SiO_2 (TWS) was used and compared with more efficient carbon oxidation carriers like CeO_2 and $Ce_{0.75}Zr_{0.25}O_2$ [17]. In particular, this work investigates $FeVO_4$ and

$Fe_{0.5}Er_{0.5}VO_4$ supported on TWS, CeO_2, $Ce_{0.75}Zr_{0.25}O_2$ ($CeZrO_2$), and Al_2O_3 in the simultaneous soot oxidation and NH_3-SCR reactions. Specific attention is given to the influence of all the components of the complex atmosphere under which these catalysts operate and to the study of the interactions between the two reactions. A promising catalytic system is proposed as a suitable candidate for both reactions.

2. Results and Discussion

2.1. Catalysts Characterization

All the samples were characterized by B.E.T. (Brunauer-Emmett-Teller) surface area measurements (reported in Table 1 and Table S1) and powder XRD analysis. As it can be observed, the specific surface area of bare supports is negatively affected by the loading of iron vanadate (B.E.T. = 4 m^2/g) and iron erbium vanadate (13 m^2/g). XRD patterns of samples made with $FeVO_4$ are reported in Figure 1A, whereas XRD diffraction patterns of supported $Fe_{0.5}Er_{0.5}VO_4$ are reported in Figure 1B. In the diffraction profile of 8.4 wt % $FeVO_4$/TWS only diffraction lines due to anatase-TiO_2 and Fe_2O_3 were observed. This is due to partial decomposition of $FeVO_4$ on TiO_2-based supports following thermal treatments [14,18]. This decomposition generates Fe_2O_3 plus VO_x species which at low coverage are not detected by XRD, while the remaining $FeVO_4$ could not be clearly identified because of superposition of its main diffraction line to the anatase main diffraction peak. In the XRD pattern of 8.4 wt % $FeVO_4/CeO_2$ instead, diffraction lines due to CeO_2, Fe_2O_3, and $CeVO_4$ are identified. In this case, the precursor $FeVO_4$ partially decomposes releasing Fe_2O_3 and VO_x species, which then react with CeO_2 already at 650 °C, resulting in the formation of $CeVO_4$ [19]. A very similar situation was detected for the 8.4 wt % $FeVO_4/Ce_{0.75}Zr_{0.25}O_2$ catalyst. The formation of surface VO_x species was confirmed by Raman spectroscopy on a representative 8.4 wt % $FeVO_4$/TWS sample calcined at 650 °C (Figure 2). We observed Raman shifts at ca. 1000 cm^{-1} that have been attributed to monomeric or dimeric species formed upon decomposition of $FeVO_4$ [20–22]. By carefully looking at different spots of the sample, also on the remaining $FeVO_4$, that were not observed by XRD, was easily detected by Raman as highlighted in Figure 2. $FeVO_4$ decomposition takes place also on alumina as revealed by Fe_2O_3 peaks in 8.4 wt % $FeVO_4/Al_2O_3$ diffraction pattern. Also in this case this is accompanied by the release of non-detectable VO_x species. Residual $FeVO_4$ species, not detectable by XRD, could be identified by Raman spectroscopy also on 8.4 wt % $FeVO_4/Al_2O_3$, as shown in Figure S1.

XRD spectra of supported $Fe_{0.5}Er_{0.5}VO_4$ (Figure 1B) are characterized by the presence of $ErVO_4$ and Fe_2O_3. It was previously highlighted that $Fe_{0.5}Er_{0.5}VO_4$ does not form a solid solution and the two vanadates ($FeVO_4$ and $ErVO_4$) are present as an intimate physical mixture [13]. The $FeVO_4$ fraction of the mixed vanadate partially decomposes releasing Fe_2O_3 and VO_x, while $ErVO_4$, which is more thermally stable than $FeVO_4$ [23], can still be detected on the various supports.

For a better understanding of the effect of the vanadate-support interaction on catalytic activity, some additional investigations were conducted also on a family of catalysts made by loading 50 wt % of vanadate on the support. Their XRD diffraction profiles are reported in Figure S2 of the supplementary material; as already noticed for 8.4 wt % $FeVO_4$ loading, the presence of Fe_2O_3 in the XRD patterns and of VO_x in Raman spectrum (Figure S3) indicates that part of $FeVO_4$ is decomposed.

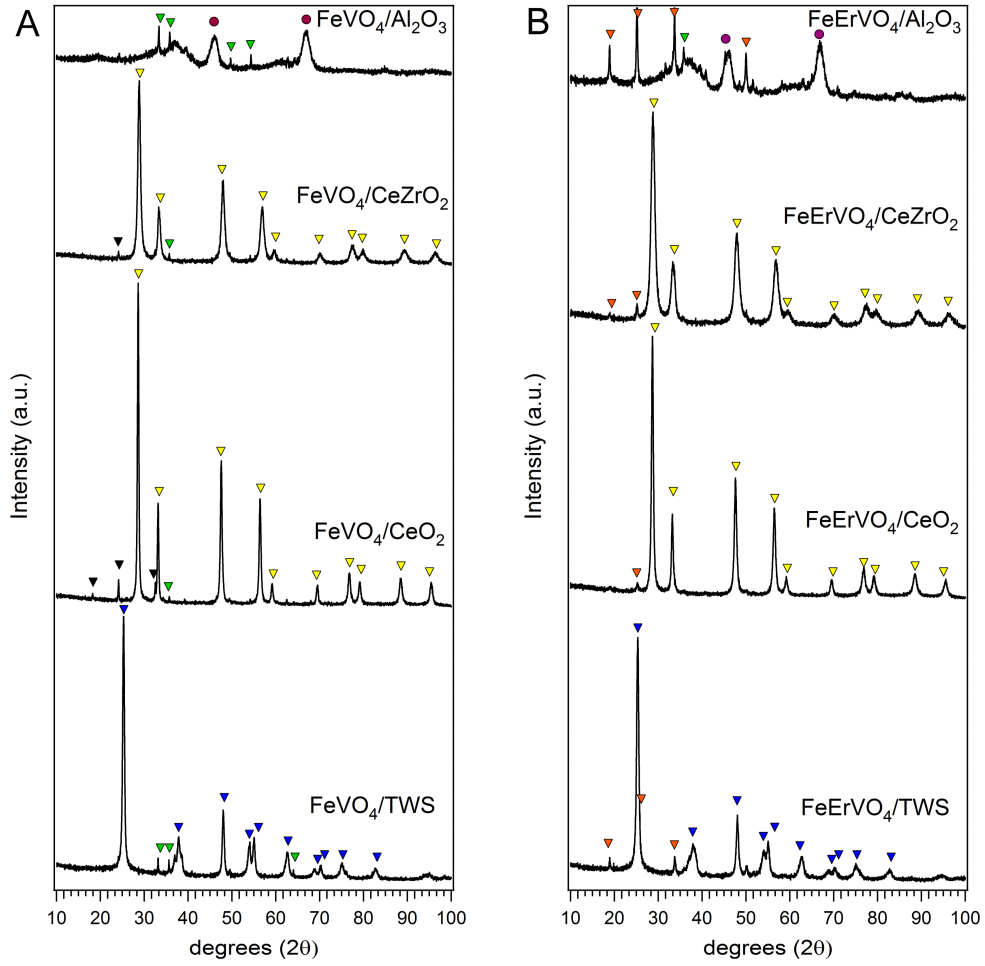

Figure 1. XRD patterns of (**A**) 8.4 wt % $FeVO_4$ and (**B**) 8.4 wt % $Fe_{0.5}Er_{0.5}VO_4$ on different supports. ▼ TiO_2-anatase, ▼ Fe_2O_3, ▼ CeO_2 or $CeZrO_2$, ▼ $CeVO_4$, ▼ $ErVO_4$, ● Al_2O_3.

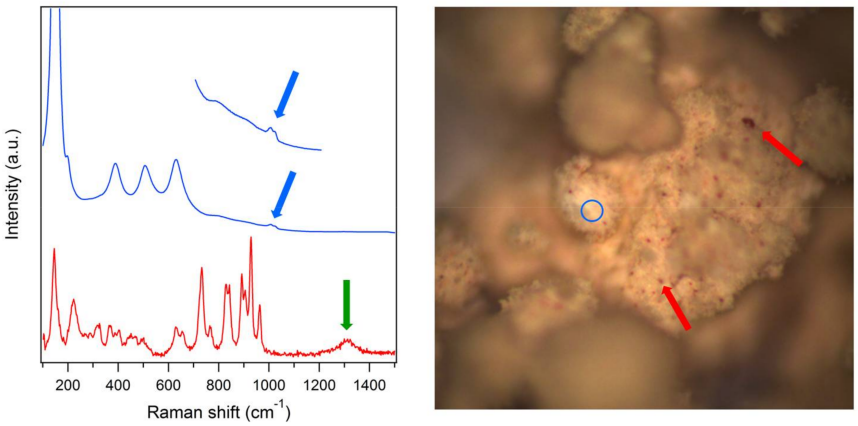

Figure 2. Raman spectra of 8.4 wt % $FeVO_4$/TWS (TiO_2-WO_3-SiO_2). The blue line represents Raman spectrum of a light spot on the sample (blue circle in the optical image) where anatase and surface VO_x (blue arrows) were detected; the red line is the spectrum of a red spot (red arrows in the optical image) showing mainly $FeVO_4$ and a band belonging to Fe_2O_3 (green arrow in the Raman spectrum).

Catalyst reducibility was measured by temperature-programmed reduction under H_2 atmosphere (TPR). Since many reducible species are involved, complex reduction profiles were obtained, as shown in Figure 3. From XRD results it is clear that $FeVO_4$ undergoes decomposition over all supports, with the formation of surface Fe_2O_3, VO_x and, on ceria-containing supports, $CeVO_4$. On Al_2O_3, which is a non-reducible support, all contributions to reduction profile are related to Fe_2O_3, VO_x, and $FeVO_4$ species. The attribution of the single TPR peaks is not straightforward, but similarly to what reported for $FeVO_4$ supported on TWS [24], the low temperature feature can be related mostly to the reduction of Fe_2O_3 and VO_x species, whereas at increasing temperature H_2 consumption due to $FeVO_4$ reduction is detected. At higher loading, an increase in hydrogen consumption is observed, which has been tentatively attributed to the residual part of $FeVO_4$, based on quantitative analysis obtained also from XRD spectra. The onset reduction temperature is independent from $FeVO_4$ initial loading (Table 1). TWS reduction profile (Figure 3A) is characterized by three reduction steps of WO_3 with the main hydrogen consumption taking place in the 800–950 °C range [25]. This feature is maintained also in the supported catalyst. Hydrogen consumption at lower temperature for 8.4 wt % $FeVO_4$/TWS (400–700 °C) is due to reduction of the supported species VO_x, Fe_2O_3, and $FeVO_4$. As for Al_2O_3 samples, it is noteworthy that the onset temperature of reduction is not related to the vanadate loading (Table 1).

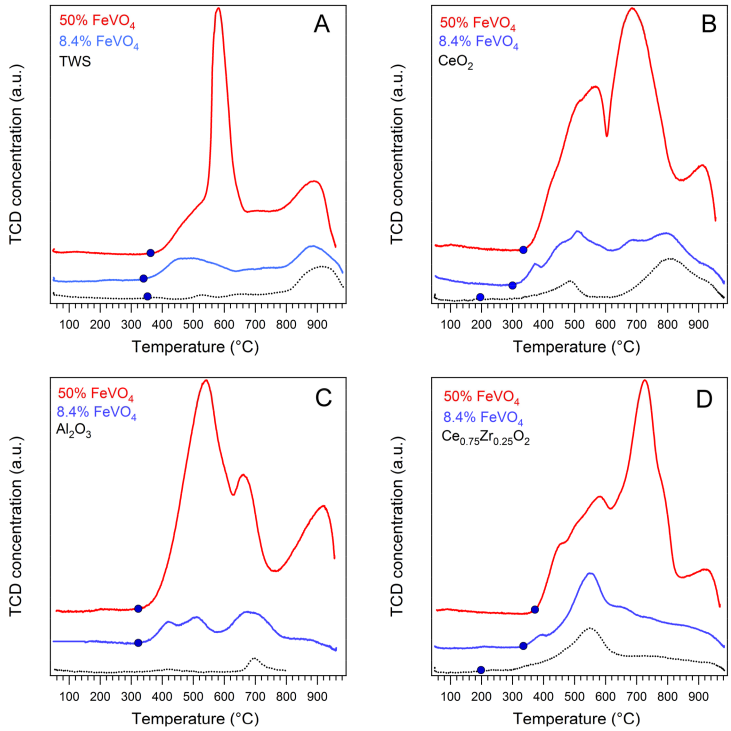

Figure 3. H_2-TPR temperature-programmed reduction under H_2 atmosphere profiles of (**A**) $FeVO_4$/TWS; (**B**) $FeVO_4/CeO_2$; (**C**) $FeVO_4/Al_2O_3$; (**D**) $FeVO_4/Ce_{0.75}Zr_{0.25}O_2$.

TPR profile of CeO_2 shows a low-T reduction feature due to surface species and a higher-T peak due to bulk reduction, as expected for pure ceria [26]. For $Ce_{0.75}Zr_{0.25}O_2$ one single hydrogen consumption peak is detected in the medium temperature range, in agreement with reported TPR profiles of ceria-zirconia solid solutions [27]. In the case of CeO_2-containing supports, a difference in the onset of the reduction can be detected at increasing $FeVO_4$ loading, in contrast to what observed for TWS and Al_2O_3-supported vanadates, indicating a strong influence of vanadate loading on sample reducibility. The temperatures of the onset of reduction are reported in Table 1 together with the overall hydrogen consumption and the H/V atomic ratio. As it can be observed from Table 1

and Figure 3, when increasing the vanadate loading up to 50 wt % the reduction peaks become more intense, the overall H_2 consumption increases but with a lower H/V ratio, indicating a better reducibility of the low-loaded samples.

Table 1. B.E.T. surface areas, hydrogen consumption in TPR, H/V atomic ratio and onset temperature of reduction for each sample.

Catalyst	B.E.T. (m^2/g)	H_2 Consumption ($mmol/g_{cat}$)	H/V Atomic Ratio [1]	Onset of Reduction (°C)
TWS	89	0.953	/	350
8.4% $FeVO_4$/TWS	68	2.184	8.88	344
50% $FeVO_4$/TWS	21	5.786	3.95	361
CeO_2	26	0.997	/	190
8.4% $FeVO_4/CeO_2$	12	1.926	7.83	285
50% $FeVO_4/CeO_2$	6	6.379	4.36	338
$Ce_{0.5}Zr_{0.5}O_2$ (CZ)	52	1.404	/	186
8.4% $FeVO_4$/CZ	24	2.448	9.95	320
50% $FeVO_4$/CZ	8	6.694	4.57	348
Al_2O_3	168	0.080	/	/
8.4% $FeVO_4/Al_2O_3$	166	1.022	4.15	320
50% $FeVO_4/Al_2O_3$	89	5.240	3.58	320

[1] Calculated on the basis of H_2 consumption from TPR profiles and total vanadium content of the catalyst.

2.2. Soot Oxidation Activity

Table 2 shows soot oxidation efficiency of the samples investigated under air atmosphere. For 8.4 wt % loaded catalysts activity under $NO/N_2/O_2$ and $NO/N_2/O_2/NH_3$ mixtures is also reported.

Soot oxidation values (T50) of the vanadates supported on TWS indicate the low efficiency of TiO_2-based materials in this reaction, as reported in the literature [17]. Compared to the oxidation potential of pure vanadates ($FeVO_4$ and $Fe_{0.5}Er_{0.5}VO_4$) supported catalysts show an increase of T50. These formulations were compared with those obtained by loading vanadates on supports that are known to be more active for soot oxidation like CeO_2 and $Ce_{0.75}Zr_{0.25}O_2$ [28].

As expected, CeO_2-based materials show lower values of T50. This can be explained through the so called "active oxygen mechanism" where, thanks to the redox ability of ceria, oxygen can be activated over a vacancy and spill over the carbon soot for oxidation [17,29,30]. Conversely, the use of redox inactive supports like Al_2O_3, results in catalyst with the highest T50. A comparison of the TPR profiles reported in Figure 3 with the corresponding onset temperatures of reduction (Table 1) evidences the correlation between sample reducibility and soot oxidation behavior. Bare CeO_2 or $Ce_{0.75}Zr_{0.25}O_2$ are the most active materials thanks to their low-temperature surface reducibility. Even with 8.4 wt % $FeVO_4$ a change in the onset temperature of reducibility of ceria is observed and, consequently, soot oxidation activity is lowered. For 50 wt % $FeVO_4/CeO_2$, the reduction is further shifted towards higher temperatures resulting in a higher soot oxidation temperature (Table 2). The opposite is obtained for TWS materials, for which an increase in $FeVO_4$ loading favours activity as no detrimental effect is displayed on reducibility in the temperature range of soot oxidation.

Table 2. Soot oxidation characteristic temperatures of investigated catalysts.

Catalyst	T50 (°C) [1] air	*Tp* (°C) [2] $NO/O_2/N_2$	*Tp* (°C) [3] $NO/O_2/N_2/NH_3$
8.4% $FeVO_4/TWS$	520	490	480
8.4% $Fe_{0.5}Er_{0.5}VO_4/TWS$	567	548	541
8.4% $FeVO_4/CeO_2$	473	459	462
8.4% $Fe_{0.5}Er_{0.5}VO_4/CeO_2$	460	448	440
8.4% $FeVO_4/CZ$	459	459	447
8.4% $Fe_{0.5}Er_{0.5}VO_4/CZ$	423	419	411
8.4% $FeVO_4/Al_2O_3$	602	-	-
8.4% $Fe_{0.5}Er_{0.5}VO_4/Al_2O_3$	603	-	-
$FeVO_4$	450	-	-
$Fe_{0.5}Er_{0.5}VO_4$	450	-	-
TWS	580	-	-
50% $FeVO_4/TWS$	474	-	-
50% $Fe_{0.5}Er_{0.5}VO_4/TWS$	449	-	-
CeO_2	390	-	-
50% $FeVO_4/CeO_2$	493	-	-
50% $Fe_{0.5}Er_{0.5}VO_4/CeO_2$	493	-	-
$CeVO_4$	495	-	-
$Ce_{0.75}Zr_{0.25}O_2$ (CZ)	385	-	-
50% $FeVO_4/CZ$	486	-	-
50% $Fe_{0.5}Er_{0.5}VO_4/CZ$	488	-	-
Al_2O_3	612	-	-
50% $FeVO_4/Al_2O_3$	546	-	-
50% $Fe_{0.5}Er_{0.5}VO_4/Al_2O_3$	505	-	-

[1] Temperature of 50% weight loss measured in thermogravimetric temperature programmed ramps from RT up to 800 °C on catalyst samples mixed in tight contact with soot. [2] Peak temperature calculated from CO_2 profiles during TPO (Temperature Programmed Oxidation) runs in a flow-trough microreactor under 500 ppm NO, 10% O_2, (balance N_2) atmosphere. [3] Peak temperature calculated from CO_2 profiles during TPO runs in a flow-trough microreactor under 500 ppm NO, 500 ppm NH_3, 10% O_2, 5% H_2O, (balance N_2) atmosphere.

These results clearly show that the mechanisms involved in soot oxidation on ceria and ceria-zirconia are different than those observed over TWS and alumina. This is better understood by looking at Figure 4 which shows the correlation between soot oxidation activity of pure and supported vanadates against loading. Similar results were obtained with $FeErVO_4$ (Supplementary material Figure S4).

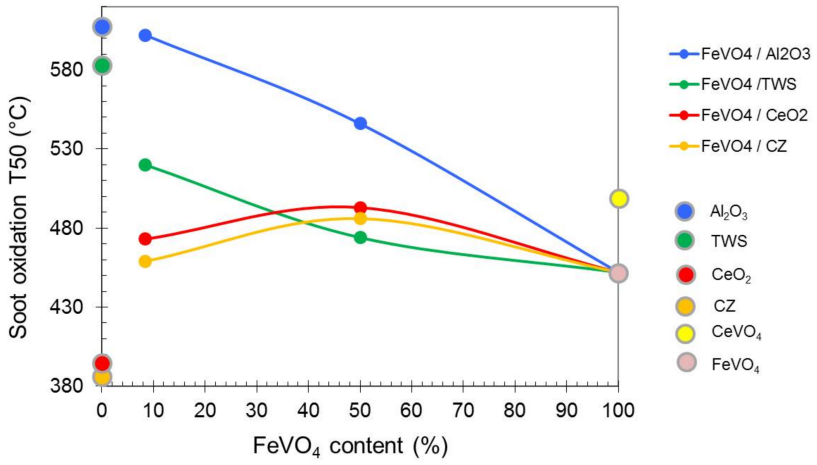

Figure 4. Effect of vanadate loading on soot oxidation activity.

For $FeVO_4$ supported on either Al_2O_3 or TWS the addition of $FeVO_4$ progressively increases activity. The effect is much more pronounced on TWS, where a strong influence is already observed at low loading. On Al_2O_3, a simple dilution effect seems to prevail, with a linear decrease in T50 going towards pure $FeVO_4$. From XRD analyses of these compounds (Figure 1 and Figure S2)

it can be observed that both in Al_2O_3 and TWS samples the decomposition of $FeVO_4$ is confirmed by the presence of Fe_2O_3 diffraction lines (corresponding VO_x were detected by Raman spectroscopy on TWS support—Figure 2 and Figure S3 in supplementary material). If on TWS the role of VO_x formed is essential for soot oxidation enhancement, $FeVO_4$ decomposition on Al_2O_3 does not have the same beneficial effect and activity is governed simply by the dilution of the catalysts components. An opposite trend is observed with CeO_2 and $Ce_{0.75}Zr_{0.25}O_2$-based materials, where the highest activity is obtained with the two bare supports; the activity then decreases reaching a minimum for the 50 wt % mixtures to increase again in correspondence of the pure vanadates. This catalytic behaviour is due to formation of $CeVO_4$ which is less active than either CeO_2 or $FeVO_4$ (Table 2). For the catalyst with a higher vanadate loading, the higher amount of $CeVO_4$ formed (Figure S2A in supplementary material), contributes to a further decrease in activity.

The effect of addition of NO and NO/NH_3 to the gas feed stream for soot oxidation was also evaluated (Table 2). In comparison to O_2/N_2 atmosphere, the presence of NO enhances soot oxidation performances of the catalysts by lowering the peak temperature due to the formation of NO_2 with its better oxidation properties compared to O_2 [31]. In a subsequent step, 500 ppm of ammonia were added to the feed gas mixture with the overall effect of slightly lowering *Tp* temperature for almost all catalysts (Table 2). The positive effect of the presence of NH_3 on soot combustion efficiency using NO_2 was observed by Tronconi et al. for Cu-Zeolite catalysts [32].

2.3. NH_3-SCR Activity

NO conversion (defined as $\{[NO_{in}] - [NO_{out}]/[NO_{in}]\}$) in the NH_3-SCR reaction was investigated for the vanadates on the different supports. Figure 5 compares their activity in the range of temperature 200–500 °C. The NO reduction profile shows a typical volcano-type shape with NO conversion increasing with temperature up to a maximum value which is reached at ca. 300–450 °C depending on the catalyst composition. At this point, the activity starts to decrease due to the ammonia oxidation reaction which is prevailing over NO reduction to N_2. The activity of supported $FeVO_4$ is higher than that of $Fe_{0.5}Er_{0.5}VO_4$ irrespective of the support used, in agreement with our earlier findings [13]. Among the different carriers, the highest activity is found with TWS, for which maximum conversions in the range 80–100% are reported. The best performing de-soot catalysts show lower activity in the standard NH_3-SCR reaction with NO conversion values in the range 45–60% at medium SCR temperatures. Al_2O_3-based catalysts are almost inactive up to 250 °C. Overall, the NO_x conversion values coupled with the better efficiency in carbon soot oxidation at lower temperature makes vanadates supported on CeO_2 and $Ce_{0.75}Zr_{0.25}O_2$ as promising catalysts to investigate the interaction between the two reactions occurring simultaneously.

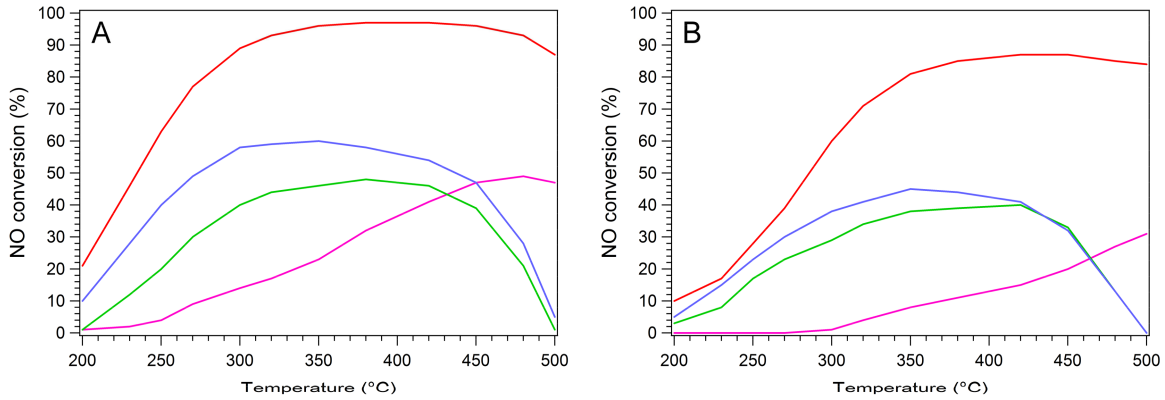

Figure 5. NO conversion in NH_3-SCR over (**A**) $FeVO_4$ (8.4 wt %) and (**B**) $Fe_{0.5}Er_{0.5}VO_4$ (8.4 wt %) loaded on different supports. Red lines: TWS, blue lines: $Ce_{0.75}Zr_{0.25}O_2$, green lines: CeO_2, magenta lines: Al_2O_3.

2.4. Simultaneous NH_3-SCR and Soot Oxidation Activity

To study the influence of soot oxidation on SCR reaction, a different set up configuration was used employing 20 mg of powder catalyst mixed in tight contact with soot. Under these conditions, the SCR reaction that is carried out at a GHSV of ca. 900,000 h^{-1} results in a lower NO_x conversion than that observed previously. This downscale of the catalytic bed was necessary to reduce pressure drop issues originating by mixing a higher amount of catalyst with soot in powder form. Figure 6 shows that for 8.4 wt % catalysts, the comparison of NO conversion obtained under the conditions described above in SCR and SCR/de-soot reaction. In addition, the CO_2 concentration profile due to soot combustion is also reported. In agreement with the results obtained with lower space velocity (Figure 5), SCR only reaction (blue curve in Figure 6), shows a typical volcano shape with a maximum conversion in the range 350–400 °C. Iron vanadates over TWS support are the best performing catalytic materials with a maximum NO conversion in the range 40–60% while a drop to lower conversion values is observed using CeO_2 and $CeZrO_2$ as supports (16–18%). In correspondence of CO_2 evolution peak, a decrease of NO conversion is observed, which is much more evident for CZ based supports. Similar results are obtained with CeO_2 (supplementary material Figure S5). NH_3 evolution profiles (not shown) reveal a decrease in NH_3 concentration in correspondence to soot oxidation that indicates a large consumption of ammonia to form NO.

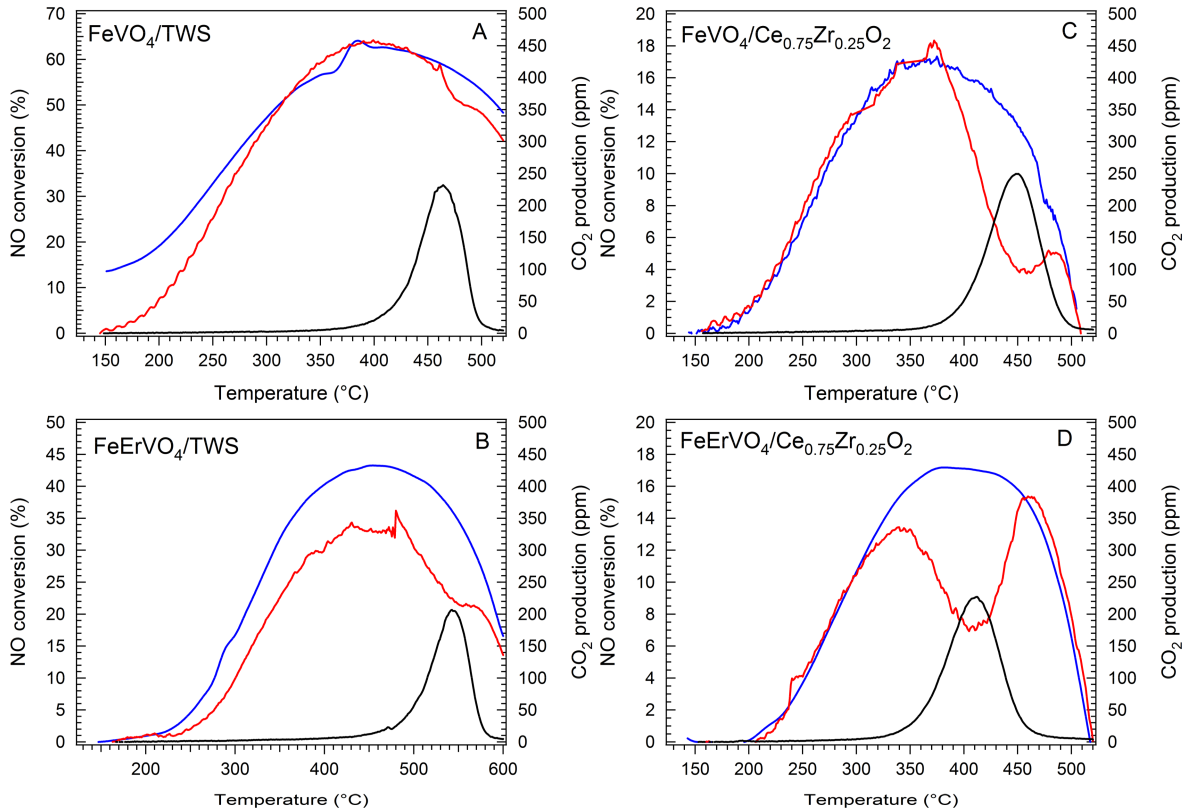

Figure 6. Comparison of 8.4 wt % loaded catalysts under the following conditions: catalyst 20 mg, NO 500 ppm, NH_3 500 ppm, O_2 10%, H_2O 5%, N_2 balance, and GHSV 900,000 h^{-1}. NO conversion in SCR (blue line), NO conversion in SCR combined with soot oxidation (red line) CO_2 evolution (black lines) (**A**) $FeVO_4$/TWS, (**B**) $FeErVO_4$/TWS, (**C**) $FeVO_4/Ce_{0.75}Zr_{0.25}O_2$, (**D**) $FeErVO_4/Ce_{0.75}Zr_{0.25}O_2$.

On pure $FeVO_4$ and $Ce_{0.75}Zr_{0.25}O_2$, negative NO conversion values are obtained (Figure 7). This indicates that NO can be generated through ammonia oxidation, and this occurs in correspondence to carbon soot oxidation. Monitoring catalyst temperature during heating ramp allowed to exclude that a local increase of temperature during carbon oxidation might affect reaction mechanism (Figure S6,

Supplementary). A similar result, that better highlights the decrease of NO conversion in SCR, is found when running the fast-SCR with NO_2 present in the feed gas on bare $Ce_{0.75}Zr_{0.25}O_2$ mixed with soot. In this case, the high NO conversion observed already at 150 °C, drops in correspondence of soot oxidation and CO_2 release (Figure 7D).

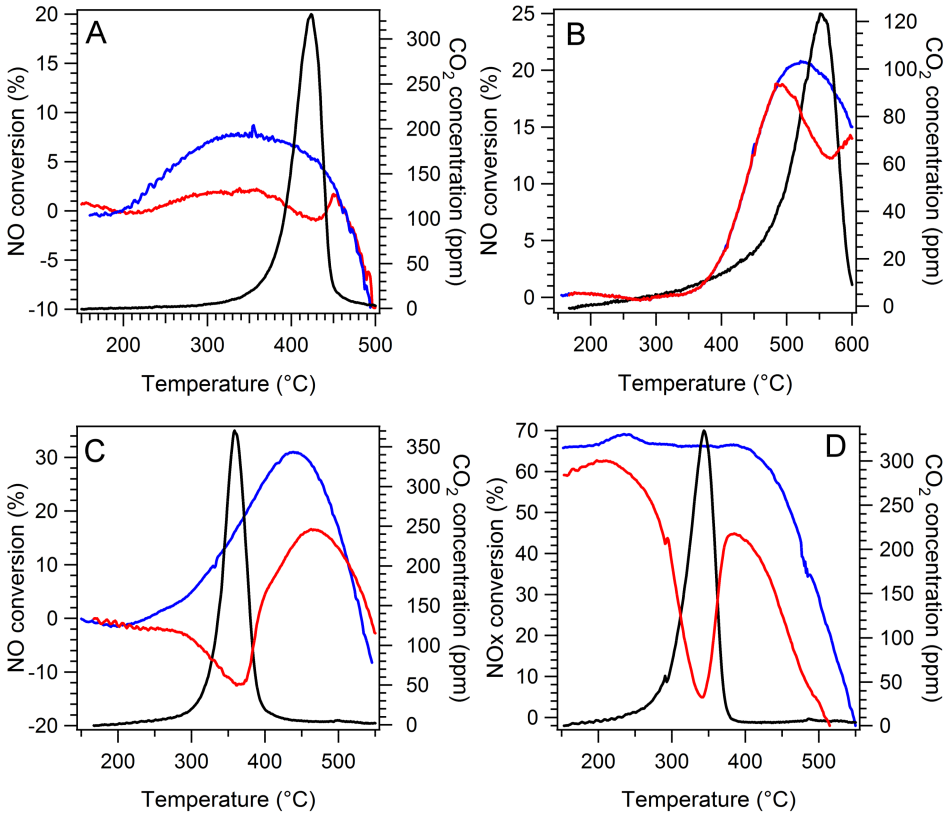

Figure 7. SCR runs on single components of the catalysts. Blue lines represent SCR of the bare samples, red lines represent SCR activity of the samples in tight contact with soot, black lines represent CO_2 production during soot combustion. (**A**) $FeVO_4$; (**B**) TWS; (**C**) $Ce_{0.75}Zr_{0.25}O_2$ standard SCR; (**D**) $Ce_{0.75}Zr_{0.25}O_2$ fast SCR.

Interestingly, a small drop in NO conversion in correspondence to soot oxidation is observed also on pure $FeVO_4$ and TWS (Figure 7A,B) which indicates that soot oxidation slightly affects NH_3-SCR also on these compounds. For this reason, ammonia oxidation reaction was studied for the single catalyst components. In Figure 8, NH_3 oxidation results over $FeVO_4$, TWS, CeO_2, $Ce_{0.75}Zr_{0.25}O_2$ are shown. The four different profiles compare reaction carried out with empty reactor, and with reactor filled with soot, catalyst and soot/catalyst mixtures. Compared to the empty reactor, soot alone has a minimal effect towards ammonia oxidation, as already observed by Mehring et al. [33]. $FeVO_4$ is the most active in the oxidation of NH_3, followed by ceria and ceria-zirconia. For $FeVO_4$, there is no large difference in NH_3 oxidation activity with or without the presence of soot. For CeO_2 and $Ce_{0.75}Zr_{0.25}O_2$ instead, the tight contact with soot (Figure 8C,D—red lines) leads to an additional NH_3 consumption in correspondence of CO_2 release due to soot combustion. This consumption is higher than the sum of contributions of catalyst and soot alone, showing a synergistic effect of the two components in NH_3 oxidation reaction and indicating that the presence of carbon soot on CeO_2 and $CeZrO_2$ produces a synergic effect increasing NH_3 oxidation to NO. No significant effect is displayed in NH_3 oxidation reaction by $CeVO_4$ which is formed on these catalysts when $FeVO_4$ is supported on CeO_2 as highlighted in Figure S7 in supplementary material. This effect is the responsible of the large decrease in NO conversion observed over ceria-containing materials in NH_3-SCR reaction.

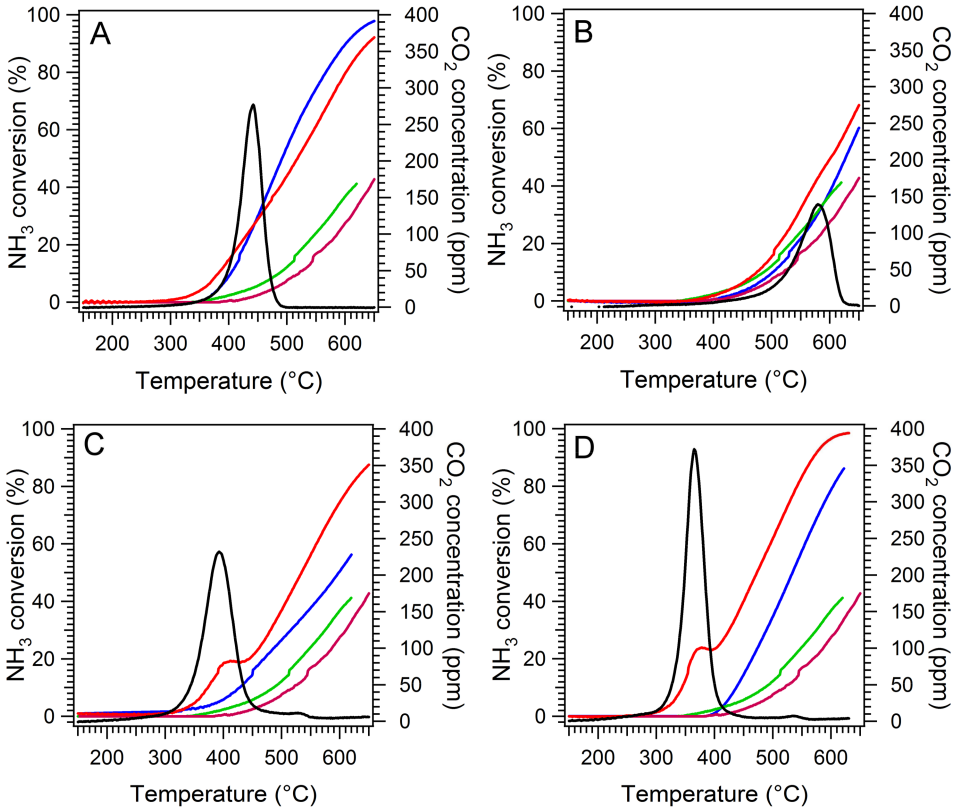

Figure 8. NH_3 oxidation carried out on single catalyst components and/or soot under the following conditions: catalyst 20 mg, NH_3 500 ppm, O_2 10%, N_2 balance, GHSV 900,000 h^{-1}. Magenta lines: NH_3 conversion curve over empty reactor; green lines: NH_3 conversion curve of bare soot; blue lines: NH_3 conversion curve over catalyst (**A**) $FeVO_4$—(**B**) TWS—(**C**) CeO_2—(**D**) $Ce_{0.75}Zr_{0.25}O_2$, red lines: NH_3 conversion over catalyst in tight contact with soot, black lines: CO_2 released during soot combustion with ongoing NH_3 oxidation reaction.

3. Experimental Section

3.1. Catalyst Preparation

$FeVO_4$ and $Fe_{0.5}Er_{0.5}VO_4$ were prepared by co-precipitation of metal nitrates ($Fe(NO_3)_3{\cdot}9H_2O$ and $Er(NO_3)_3{\cdot}6H_2O$, Treibacher Industrie AG, Althofen, Austria)) and ammonium metavanadate (99+%, Sigma-Aldrich, St. Louis, MO, USA). Aqueous solutions of the precursors were separately prepared at 80 °C. After unification, the pH was adjusted by means of ammonia (28% aqueous solution, Sigma-Aldrich) to obtain the respective precipitate which was filtered, washed and dried at 120 °C overnight. These vanadates were subsequently used to make the supported catalysts. All support used in this study were commercial materials (CeO_2 from Treibacher Industrie AG, $CeZrO_2$ from W.R. Grace (Columbia, MD, USA), TWS from Cristal (Hong Kong, China), Al_2O_3 from Sasol Germany GmbH (Hamburg, Germany)). Supported catalysts were prepared by mixing two separate aqueous slurries containing, respectively, the vanadate and the support. Vanadate/support weight ratio was 8.4/91.6 or 50/50. Combined slurries were evaporated to dryness. The resulting solids were dried at 120 °C overnight followed by calcination at 650 °C/2 h in a muffle furnace to obtain the final catalyst.

3.2. Catalytic Tests

Soot combustion efficiency under air was measured by means of thermogravimetry using soot (Printex U-Degussa)/catalyst mixtures under tight contact conditions obtained by mixing the two components in an agate mortar for 10 min. The soot/catalyst weight ratio was 1:20. The samples were placed on Pt crucibles licked by air flow (60 mL/min) and heated at a constant rate of 10 °C/min from RT up to 800 °C. T50 values, corresponding to the temperature at which 50 wt % of carbon is lost, was used as a measure of soot oxidation activity. Soot oxidation under $NO/O_2/N_2$ and $NO/O_2/N_2/NH_3$ was carried out in a laboratory set-up equipped with a quartz microreactor for powder testing. In these experiments 20 mg of sample in powder form (soot/catalyst ratio of 20:1, mixed in tight contact) were exposed to a 300 mL/min feed stream of composition 500 ppm NO, 500 ppm NH_3 (when present), 10% O_2, 5% H_2O, balance N_2 with a GHSV of 900,000 h^{-1}.

NH_3-SCR activity was measured in the same laboratory set-up described above on 100 mg of catalyst pressed and sieved ($350 < Ø < 425$ μm) under a 300 mL/min feed stream of composition 500 ppm NO, 500 ppm NH_3, 10% O_2, 5% H_2O, balance N_2 with a GHSV of 180,000 h^{-1}.

NH_3 oxidation experiments were conducted on 20 mg catalytic beds under a reactive atmosphere of composition 500 ppm NH_3, 10% O_2, balance N_2 with a GHSV of 900,000 h^{-1}. Ammonia concentration was monitored during a temperature ramp from 150 °C up to 650 °C. When soot was present, also CO_2 release due to carbon oxidation was monitored.

For all experiment conducted in the gas bench, the composition of the feed stream (reagents and products) was analyzed with an on line MKS 2030 MultiGas Analyzer FT-IR instrument.

3.3. Characterization of the Catalysts

Specific surface areas of catalysts were measured by nitrogen adsorption at -196 °C according to the B.E.T. method on a Tristar 3000 gas analyzer (Micromeritics, Norcross, GA, USA). Prior to the measurement all samples were outgassed at 150 °C for 1.5 h. Powder X-ray diffraction patterns were collected on a Philips X'Pert diffractometer (PANalytical B.V., Almelo, The Netherlands) operated at 40 kV and 40 mA using Ni filtered Cu Kα radiation. Data were recorded from 10 to 100° 2θ using a step size of 0.02° and a counting time of 40 s per angular abscissa. Phase identification was conducted with the Philips X'Pert Highscore software (PANalytical B.V., Almelo, The Netherlands, 2002). Reducibility of the samples was measured by temperature programmed reduction (TPR) runs; approximately 50 mg of samples were heated at 10 °C/min in a U-shaped quartz reactor from room temperature up to 960 °C under a 4.5 vol % H_2/N_2 flow (35 mL/min). The samples were pretreated at 500 °C for 1 h under air flow. Hydrogen consumption was monitored with a thermal conductivity detector (TCD) in an Autochem II 2920 instrument (Autochem II 2920, Micromeritics, Norcross, GA, USA). Raman spectra were collected with a Xplora Plus Micro-Raman system (Horiba, Kyoto, Japan) equipped with a cooled CCD detector (−60 °C) and Edge filter. The samples were excited with the 512 nm radiation in a Linkam CR1000 in situ cell at 200 °C under flowing air. The spectral resolution was 1 cm^{-1} and the spectra acquisition was of 5 accumulations of 10 or 20 s with a 50× LWD objective. The optical images were collected with an integrated microscope Olympus BX43 (Olympus, Tokyo, Japan) with a 10× objective.

4. Conclusions

A systematic screening to evaluate the interaction between soot oxidation and NH_3-SCR has been carried out investigating the behavior of $FeVO_4$ and $Fe_{0.5}Er_{0.5}VO_4$ loaded on standard SCR supports like TiO_2-WO_3-SiO_2, redox active carriers like CeO_2 or $Ce_{0.75}Zr_{0.25}O_2$ and Al_2O_3.

It is shown by combined XRD, TPR, and Raman spectroscopy that vanadates partially decompose over TiO_2-based materials and Al_2O_3 with formation of Fe_2O_3 and surface VO_x species. In the presence of $CeO_2/CeZrO_2$, formation of crystalline $CeVO_4$ along with Fe_2O_3 is reported.

Al_2O_3-based materials are almost inactive either in SCR and soot oxidation while, as expected, TiO_2-based materials are highly active in NH_3-SCR and $CeO_2/CeZrO_2$ are active in carbon soot oxidation. The addition of ammonia is found to slightly influence soot oxidation by reducing its combustion temperature by a few degrees while the presence of soot is found to affect SCR reaction, especially in the presence of CeO_2 and $CeZrO_2$. This is due to the combined effect of the catalyst and carbon soot that results in an enhancement of NH_3 oxidation reaction.

Supplementary Materials: The following are available online at http://www.mdpi.com/2073-4344/8/4/130/s1, Figure S1: Raman spectra of 8.4 wt % $FeVO_4/Al_2O_3$. In the blue line (grating 1800 L/mm with 5 s per accumulation) only Fe_2O_3 and Al_2O_3 Raman shifts are visible. Surface VO_x could not be detected. In the red line Raman shifts mainly attributable to $FeVO_4$ and Fe_2O_3 are shown, Figure S2: XRD patterns of (A) 50 wt % $FeVO_4$ and (B) 50 wt % $FeErVO_4$ on different supports. Figure S3: Raman spectra of 50 wt % $FeVO_4$/TWS. The optical image of the sample shows that the dark spots of $FeVO_4$ and Fe_2O_3 are uniformly distributed and all Raman spectra show the Raman shifts of $FeVO_4$. Figure S4: Effect of $FeErVO_4$ loading on soot oxidation activity, Figure S5: Comparison of SCR catalytic activity of 20 mg catalytic beds of bare catalysts and with soot oxidation conducted simultaneously, Figure S6: Comparison between theoretical heating ramp and temperature measured in the catalyst bed during soot oxidation reaction on CeO_2 sample (tight contact, soot/catalyst weight ratio of 1:20), Figure S7: NH_3 oxidation carried out on single catalyst components under the following conditions: catalyst 20 mg, NH_3 500 ppm, O_2 10%, N_2 balance, GHSV 900,000 h^{-1}, Table S1: B.E.T. surface areas of $Fe_{0.5}Er_{0.5}VO_4$ catalysts.

Acknowledgments: Authors would like to thank Interreg V Italy-Austria project Coat4Cata (project n. ITAT 1019) for funding, for research support and for covering the costs to publish in open access.

Author Contributions: M.C. and A.T. conceived and designed the experiments; M.C. performed the experiments; M.C., S.C., and A.T. analyzed the data; A.T. contributed reagents/materials/analysis tools; M.C. prepared tables and figures and wrote the first draft of the manuscript and S.C. and A.T. contributed to subsequent revisions. All authors agreed to the final version of the paper.

Conflicts of Interest: The authors declare no conflict of interest.

References

1. Bassou, B.; Guilhaume, N.; Iojoiu, E.E.; Farrusseng, D.; Lombaert, K.; Bianchi, D.; Mirodatos, C. High-throughput approach to the catalytic combustion of diesel soot II: Screening of oxide-based catalysts. *Catal. Today* **2011**, *159*, 138–143. [CrossRef]
2. Granger, P.; Parvulescu, V.I. Catalytic NO_x abatement systems for mobile sources: From three-way to lean burn after-treatment technologies. *Chem. Rev.* **2011**, *111*, 3155–3207. [CrossRef] [PubMed]
3. Liu, Z.M.; Woo, S.I. Recent advances in catalytic deNO($_x$) science and technology. *Catal. Rev.* **2006**, *48*, 43–89. [CrossRef]
4. Brandenberger, S.; Krocher, O.; Tissler, A.; Althoff, R. The state of the art in selective catalytic reduction of NO_x by ammonia using metal-exchanged zeolite catalysts. *Catal. Rev.* **2008**, *50*, 492–531. [CrossRef]
5. Boger, T. Integration of SCR functionality into diesel particulate filters. In *Urea-Scr Technology for Denox after Treatment of Diesel Exhausts*; Nova, I., Tronconi, E., Eds.; Springer: New York, NY, USA, 2014; pp. 623–655.
6. Johnson, T.V. Review of selective catalytic reduction (SCR) and related technologies for mobile applications. In *Urea-SCR Technology for deNO$_x$ after Treatment of Diesel Exhausts*; Nova, I., Tronconi, E., Eds.; Springer: New York, NY, USA, 2014; pp. 3–31.
7. Weibel, M.; Waldbusser, N.; Wunsch, R.; Chatterjee, D.; Bandl-Konrad, B.; Krutzsch, B. A novel approach to catalysis for NO_x reduction in diesel exhaust gas. *Top. Catal.* **2009**, *52*, 1702–1708. [CrossRef]
8. Watling, T.C.; Ravenscroft, M.R.; Avery, G. Development, validation and application of a model for an SCR catalyst coated diesel particulate filter. *Catal. Today* **2012**, *188*, 32–41. [CrossRef]
9. Song, X.; Johnson, J.H.; Naber, J.D. A review of the literature of selective catalytic reduction catalysts integrated into diesel particulate filters. *Int. J. Engine Res.* **2015**, *16*, 738–749. [CrossRef]
10. Cavataio, G.; Warner, J.R.; Girard, J.W.; Ura, J.; Dobson, D.; Lambert, C.K. Laboratory study of soot, propylene and diesel fuel impact on zeolite-based SCR filter catalysts. *SAE Int. J. Fuels Lubr.* **2009**, *2*, 342–368. [CrossRef]
11. Casanova, M.; Schermanz, K.; Llorca, J.; Trovarelli, A. Improved high temperature stability of NH_3-SCR catalysts based on rare earth vanadates supported on TiO_2-WO_3-SiO_2. *Catal. Today* **2012**, *184*, 227–236. [CrossRef]

12. Vargas, M.A.L.; Casanova, M.; Trovarelli, A.; Busca, G. An IR study of thermally stable V_2O_5-WO_3-TiO_2 SCR catalysts modified with silica and rare-earths (Ce, Tb, Er). *Appl. Catal. B Environ.* **2007**, *75*, 303–311. [CrossRef]
13. Casanova, M.; Llorca, J.; Sagar, A.; Schermanz, K.; Trovarelli, A. Mixed iron-erbium vanadate NH_3-SCR catalysts. *Catal. Today* **2015**, *241*, 159–168. [CrossRef]
14. Marberger, A.; Elsener, M.; Ferri, D.; Sagar, A.; Schermanz, K.; Krocher, O. Generation of NH_3 selective catalytic reduction active catalysts from decomposition of supported $FeVO_4$. *ACS Catal.* **2015**, *5*, 4180–4188. [CrossRef]
15. Liu, F.; He, H.; Lian, Z.; Shan, W.; Xie, L.; Asakura, K.; Yang, W.; Deng, H. Highly dispersed iron vanadate catalyst supported on TiO_2 for the selective catalytic reduction of NO_x with NH_3. *J. Catal.* **2013**, *307*, 340–351. [CrossRef]
16. Gillot, S.; Tricot, G.; Vezin, H.; Dacquin, J.-P.; Dujardin, C.; Granger, P. Development of stable and efficient $CeVO_4$ systems for the selective reduction of NO_x by ammonia: Structure-activity relationship. *Appl. Catal. B Environ.* **2017**, *218*, 338–348. [CrossRef]
17. Bueno-Lopez, A. Diesel soot combustion ceria catalysts. *Appl. Catal. B Environ.* **2014**, *146*, 1–11. [CrossRef]
18. Casanova, M.; Nodari, L.; Sagar, A.; Schermanz, K.; Trovarelli, A. Preparation, characterization and NH_3-SCR activity of $FeVO_4$ supported on TiO_2-WO_3-SiO_2. *Appl. Catal. B Environ.* **2015**, *176*, 699–708. [CrossRef]
19. Wu, Z.L.; Rondinone, A.J.; Ivanov, I.N.; Overbury, S.H. Structure of vanadium oxide supported on ceria by multiwavelength raman spectroscopy. *J. Phys. Chem. C* **2011**, *115*, 25368–25378. [CrossRef]
20. Went, G.T.; Leu, L.J.; Bell, A.T. Quantitative structural-analysis of dispersed vanadia species in TiO_2(anatase)-supported V_2O_5. *J. Catal.* **1992**, *134*, 479–491. [CrossRef]
21. Wachs, I.E. Raman and IR studies of surface metal oxide species on oxide supports: Supported metal oxide catalysts. *Catal. Today* **1996**, *27*, 437–455. [CrossRef]
22. Haber, J.; Machej, T.; Serwicka, E.M.; Wachs, I.E. Mechanism of surface spreading in vanadia-titania system. *Catal. Lett.* **1995**, *32*, 101–114. [CrossRef]
23. Gaur, K.; Lal, H.B. Electrical transport in heavy rare-earth vanadates. *J. Mater. Sci.* **1986**, *21*, 2289–2296. [CrossRef]
24. Casanova, M.; Sagar, A.; Schermanz, K.; Trovarelli, A. Enhanced stability of Fe_2O_3-doped $FeVO_4/TiO_2$-WO_3-SiO_2 SCR catalysts. *Top. Catal.* **2016**, *59*, 996–1001. [CrossRef]
25. Vermaire, D.C.; Vanberge, P.C. The preparation of WO_3/TiO_2 and WO_3/Al_2O_3 and characterization by temperature-programmed reduction. *J. Catal.* **1989**, *116*, 309–317. [CrossRef]
26. Giordano, F.; Trovarelli, A.; de Leitenburg, C.; Giona, M. A model for the temperature-programmed reduction of low and high surface area ceria. *J. Catal.* **2000**, *193*, 273–282. [CrossRef]
27. Daturi, M.; Finocchio, E.; Binet, C.; Lavalley, J.-C.; Fally, F.; Perrichon, V.; Vidal, H.; Hickey, N.; Kašpar, J. Reduction of high surface area CeO_2-ZrO_2 mixed oxides. *J. Phys. Chem. B* **2000**, *104*, 9186–9194. [CrossRef]
28. Gallert, T.; Casanova, M.; Puzzo, F.; Strazzolini, P.; Trovarelli, A. SO_2 resistant soot oxidation catalysts based on orthovanadates. *Catal. Commun.* **2017**, *97*, 120–124. [CrossRef]
29. Machida, M.; Murata, Y.; Kishikawa, K.; Zhang, D.J.; Ikeue, K. On the reasons for high activity of CeO_2 catalyst for soot oxidation. *Chem. Mater.* **2008**, *20*, 4489–4494. [CrossRef]
30. Soler, L.; Casanovas, A.; Escudero, C.; Pérez-Dieste, V.; Aneggi, E.; Trovarelli, A.; Llorca, J. Ambient pressure photoemission spectroscopy reveals the mechanism of carbon soot oxidation in ceria-based catalysts. *ChemCatChem* **2016**, *8*, 2748–2751. [CrossRef]
31. Zouaoui, N.; Issa, M.; Kehrli, D.; Jeguirim, M. CeO_2 catalytic activity for soot oxidation under NO/O_2 in loose and tight contact. *Catal. Today* **2012**, *189*, 65–69. [CrossRef]
32. Tronconi, E.; Nova, I.; Marchitti, F.; Koltsakis, G.; Karamitros, D.; Maletic, B.; Markert, N.; Chatterjee, D.; Hehle, M. Interaction of NO_x reduction and soot oxidation in a DPF with Cu-Zeolite SCR coating. *Emiss. Control Sci. Technol.* **2015**, *1*, 134–151. [CrossRef]
33. Mehring, M.; Elsener, M.; Kröcher, O. Selective catalytic reduction of NO_x with ammonia over soot. *ACS Catal.* **2012**, *2*, 1507–1518. [CrossRef]